CYCLIC BEHAVIOUR OF THE SINGLE CRYSTAL SUPERALLOY SRR99 AT 980°C

P.D. Portella, A. Bertram, E. Fahlbusch, H. Frenz and J. Kinder

Federal Institute of Materials Research and Testing (BAM)
Unter den Eichen 87, D-12205 Berlin, FRG

ABSTRACT

[001]-oriented specimens of the single crystal superalloy SRR99 were subjected to different stress- and strain-controlled cyclic loading tests (cyclic creep, LCF, LCF with hold times under tensile or compressive loading) at 980°C. The observed mechanical behaviour is discussed considering the microstructural evolution and, in some cases, the damage evolution in the course of the experiments. A visco-elastic model used to successfully describe the behaviour of SRR99 under cyclic loading conditions allows a precise estimate of specimens lifetime.

KEYWORDS

SRR99; single crystal superalloy; cyclic behaviour; cyclic creep; LCF; microstructural evolution; damage evolution; modelling; lifetime prediction.

CYCLIC CREEP

Different cyclic creep experiments have been carried out on SRR99 specimens at 980°C. The upper tensile load (σ_u) was kept constant at 200 MPa, the upper hold time was varied between 10 s and 300 s. The lower load (σ_l) was chosen between -200 MPa and 180 MPa with the same hold times. In most cases, the hold times for both stress levels were symmetrical, but in certain cases an asymmetrical time division was applied. The alternating stress levels led to values of $R = \sigma_l / \sigma_u$ ranging from -1 to 0.8. Usually, the experiments were conducted to a maximum strain of approximately 5 % or until a total experimental time of 500 hours. The results of these experiments are presented in Fig. 1, which also shows the monotonous creep behaviour of SRR99 at 200 MPa (R = 1).

In the experiments with $0 < R < 1$ and a symmetrical load cycle we observed both a decrease in creep strain rate and an increase in lifetime, which become more pronounced by decreasing R. On the other hand, a reduction in the lower hold time leads to an increase in the creep strain rate, as shown in Fig. 1 for R = 0.1. In all these experiments we observed backward creep strain in the σ_l-phase. Hence, the internal stress built up in the σ_u-phase is high enough to promote the backflow of the mobile dislocations and the specimen contraction in the σ_l-phase. A similar effect was observed in other strongly particle-hardened materials as in the ODS-alloy MA 754 (Thien *et al.*, 1981).

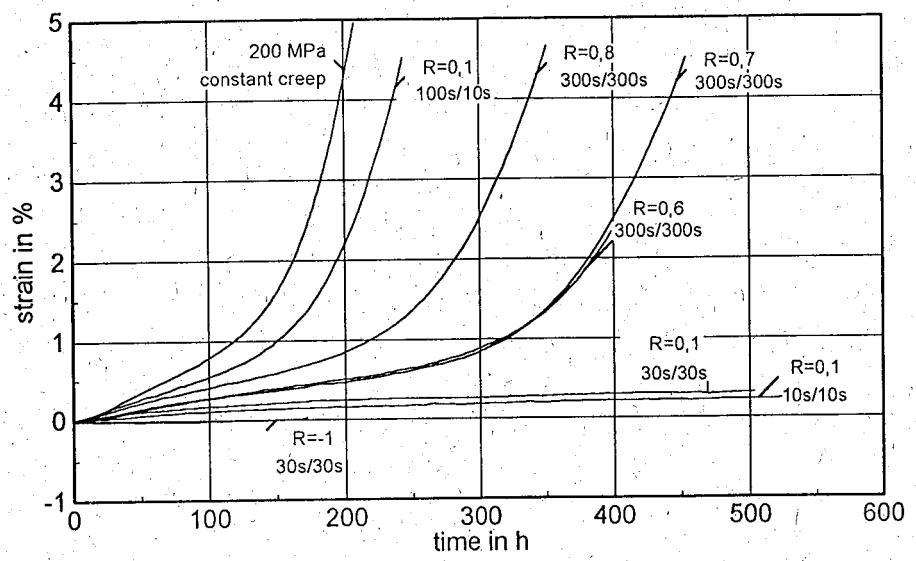

Fig. 1. Cyclic and monotonous creep curves of SRR99 at 980°C and for σ_u = 200 MPa. Upper and lower hold times are given for each test.

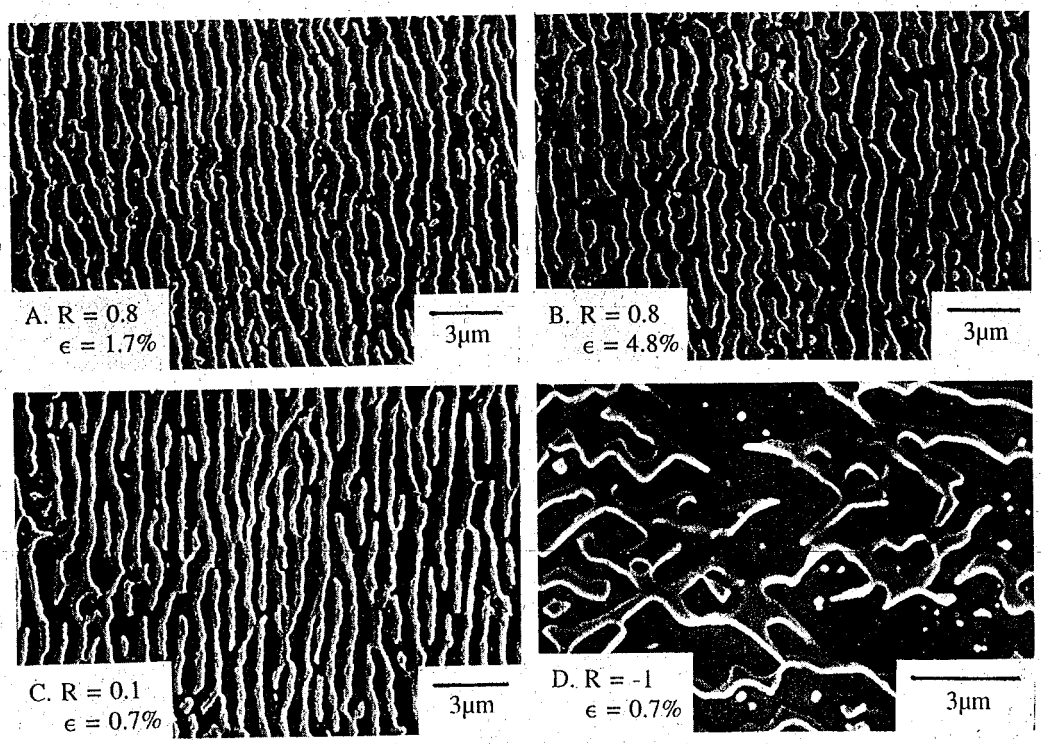

Fig. 2. γ/γ'-microstructure after cyclic creep loading. (010) longitudinal sections

The evolution of the γ/γ'-microstructure for R-values between 0 and 1 is shown in Fig. 2. The initial cuboidal microstructure was altered after relatively low creep strain into a lamellar one, the lamellae lying perpendicular to the stress direction. With increasing strain these lamellae became smaller, *i.e.* the mean length of their section in the metallographic specimens decreased significantly. Further, we measured a slight decrease of the area fraction of γ' from about 60% to 50%. This result was independent of the orientation of the metallographic section, so that we may assume the same reduction in the volume fraction of γ'. Under monotonous creep conditions we observed a very similar microstructural evolution.

The experiments with R = -1 led to the fracture of the specimens after very small plastic deformation, the maximum strain in the last cycle ranging between - 0.37 % and 0.5 %. Under these conditions the γ' cube-like particles seem to change to folded plates lying mainly parallel to ((111)) planes, Fig. 2. For this γ/γ'-microstructure we measured different values of the γ' area fraction depending on the orientation of the metallographic section.

LOW CYCLE FATIGUE

LCF-tests were performed under total strain control and a triangular wave form (Portella and Kinder, 1995). Independently of the strain amplitude, $\Delta\epsilon_t$, we observed for a strain rate of 10^{-3} s^{-1} a slight softening in the very first cycles followed by a much slower reduction in the stress amplitude, $\Delta\sigma$, Fig. 3. The faster reduction in the last cycles is due to the growth of surface cracks. In all these experiments there was only a faint change in the γ/γ'-microstructure. On the other hand, LCF-tests with a strain rate of 10^{-5} s^{-1} led to a slight softening in the first cycles followed by a much more pronounced reduction in $\Delta\sigma$. The γ/γ'-microstructure observed in this case after 16 cycles is very similar to that observed after the same test time at the end of the experiment with 10^{-3} s^{-1}. The continuous softening observed afterwards is accompanied by the coarsening of the γ'-phase to folded plates lying mainly parallel to ((111)) planes, a similar structure to that observed in experiments with $R_\sigma = -1$.

The fracture mechanism under LCF loading was independent of the strain rate. A large population of small surface cracks perpendicular to the specimen axis could be observed at $N \approx \frac{1}{2} N_f$. These cracks were induced by oxidation, whereas their microstructural origin could not be identified. Some of the cracks coalesced to form the main crack, which grew perpendicular to the specimen axis. This last stage was responsible for the very last part of the $\Delta\sigma$ x N diagram, whose form depends on the relative position of main crack and extensometer.

The effect of relaxation periods on the LCF behaviour of this alloy was investigated by holding the strain for 300 s either at the maximum strain level, *i.e.* in the tension phase, or at the minimum strain level, *i.e.* in the compression phase.

Hold times in the compression phase led to a reduction in N_f by a factor of about 2 for $\Delta\epsilon_t = 1.2$ % in comparison to the lifetime under LCF loading. This reduction factor even increases by decreasing $\Delta\epsilon_t$. The evolution of the γ/γ'-microstructure is dictated by the compression stress during the hold times with the formation of γ plates on ((100)) planes parallel to the specimen axis. Fracture under these loading conditions is initiated by the same type of surface cracks, as reported above for LCF loading. The main crack, however, grows from both ends of a such surface crack on two ((111)) planes.

A reduction in N_f by a factor of about 2 is also observed when introducing a hold time of 300 s in the

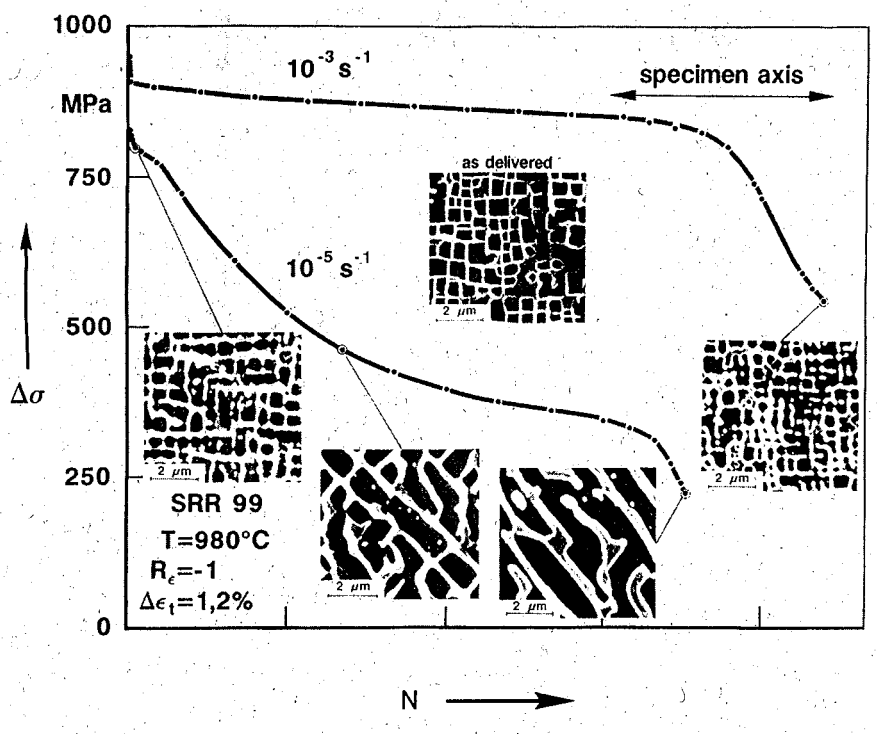

Fig. 3. Microstructural evolution during LCF-tests without hold times for two values of the total strain rate.

tension phase for $\Delta\epsilon_t$ = 1.2 %. Decreasing the strain amplitudes leads under these loading conditions to a decrease in the reduction factor and even to larger lifetimes than those observed under LCF loading. Both the evolution of the γ/γ'-microstructure and the fracture mechanism are governed by the tension stress during the hold times, *viz.* with the formation of γ plates lying perpendicular to the specimen axis and with the growth of creep cracks from micropores in the bulk of the specimens. These creep cracks grow perpendicular to the specimen axis and assume a square shape with the sides parallel to [[110]] directions. The final fracture is a result of the connection of a large number of creep cracks by shearing of the ligaments.

MODELLING

Bertram *et al.* (1991, 1993) used a Burgers-type model combined with a Kachanov / Rabotnov damage variable to describe the high temperature creep behaviour of SRR99. This model also allows the description of the cyclic behaviour of SRR99 at 980°C under either stress- or strain-controlled conditions using a single set of material parameters (Bertram and Fahlbusch, 1995).

For the description of the damage under cyclic loading, the evolution equation for creep damage was extended according to the Franklin/Danzer rule (Aktaa *et al.*, 1993; Rubeša and Danzer, 1994). The evolution equation for damage variable, δ, takes the following form

$$\dot{\delta} = C_{D3}\frac{\sigma_0(t)^{C_{D1}}}{(1-\delta(t))^{C_{D2}}}\left|\frac{\dot{\epsilon}_{in}(t)}{C_{D5}\,\epsilon_{c,min}(t)}\right|^{C_{D4}}, \qquad \dot{\epsilon}_{c,min}(t) = \frac{\sigma_0(t)}{L(\sigma(t))},$$

where σ_0 is the nominal stress and L is one of the viscosities of the model which are dependent on the effective stress σ (Bertram and Fahlbusch, 1995). The damage parameters C_{D1}, C_{D2}, C_{D3} and C_{D5} can be determined by creep tests, C_{D4} by LCF-tests.

This model was fitted using four creep tests as well as the first cycle of three LCF tests without hold time. Figures 4 and 5 show the creep- and LCF-tests which were used for the calibration. The symbols represent some of the experimental values and the lines the curves calculated using this set of parameters. Figures 6 and 7 show the experimental values (symbols) of some tensile (CERT) and cyclic creep tests and the corresponding calculated curves using the same set of parameters. Finally, Figs. 8 and 9 show the comparison of the observed lifetime of specimens (symbols) and the estimates obtained from the model (line) for strain-controlled LCF and creep tests. First results of the lifetime prediction for specimens submitted to LCF-loading with hold times are in good agreement with the experimental results.

ACKNOWLEDGEMENTS

This work was partially suported by the Bundesministerium für Forschung und Technologie, BMFT, contract number 03 M3038 D. The authors are indebted for the contributions of Monique Dugué-peroux and Jens Riedel.

REFERENCES

Aktaa, J., D. Munz and B. Schinke (1993). The dependence of damage on internal variables and its incorporation into constitutive equations. In: *Transactions of SMIRT-12* (K. Kussmaul, ed.), 135-140. Elsevier Science Publishers, Oxford.

Bertram, A., J. Olschewski, M. Zelewski and R. Sievert (1991). Anisotropic creep modeling for F.C.C. single crystals. In: *Proc. IUTAM Symp. "Creep in Structures IV"* (M. Zyczkowski, ed.), 29-36. Springer, Berlin.

Bertram, A., J. Olschewski, R. Sievert and M. Zelewski (1993). Creep modelling and lifetime prediction for nickel-base single crystals at high temperatures. In: *Transactions of SMIRT-12* (K. Kussmaul, ed.), 147-151. Elsevier Science Publishers, Oxford.

Bertram, A. and E. Fahlbusch (1995). Einachsige Materialmodellierung von Superlegierungen im Hochtemperaturbereich. BAM-V.31 Technical Report. Bundesanstalt für Materialforschung und -prüfung, Berlin.

Portella, P.D., and J. Kinder (1995). Microstructural evolution during creep and LCF-testing of single crystal superalloy SRR99. Submitted to *Materials Science and Engineering A*.

Rubeša, D. and R. Danzer (1994). Reevaluation of the SRM lifetime prediction rule by coupling it with a suitable constitutive model. In: *Localized Damage III: Computer-Aided Assessment and Control* (M.H. Aliabadi *et al.*, eds.). Computational Mechanics Publications, Southampton/Boston.

Thien, J.K., D.E. Matejczyk, Y. Zhuang and T.E. Howson (1981). Anelastic relaxation, cyclic creep and stress rupture of γ' and oxide dispersion strengthened superalloys. In: *Creep and fracture of engineering materials and structures* (B. Wilshire and D.R.J. Owen, eds.), 433-446. Pineridge Press, Swansea.

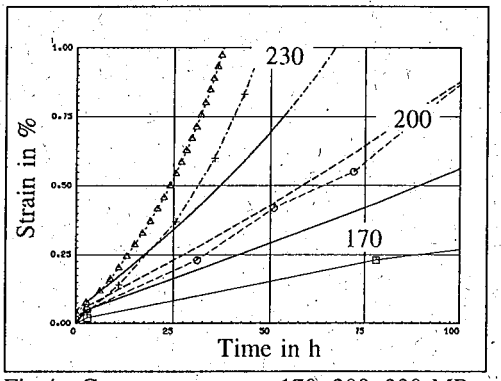

Fig.4. Creep tests at σ_0= 170, 200, 230 MPa.

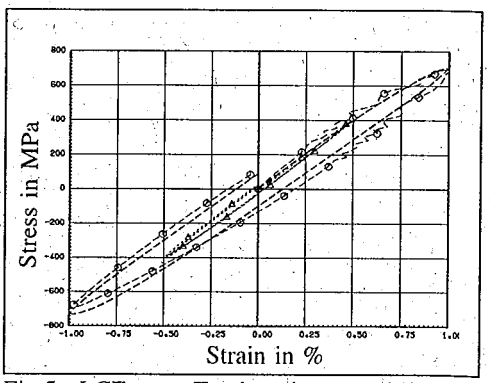

Fig.5. LCF tests. Total strain range 2%, 1%.

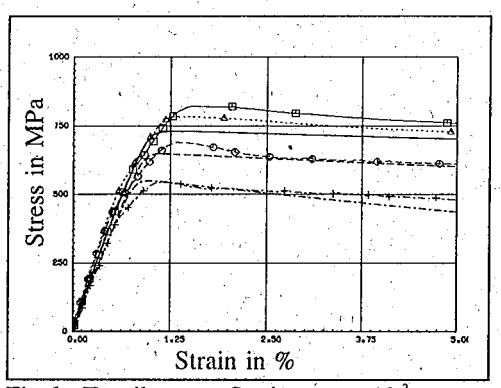

Fig.6. Tensile tests. Strain rate at 10^{-3}, 10^{-4}, 10^{-5} 1/s.

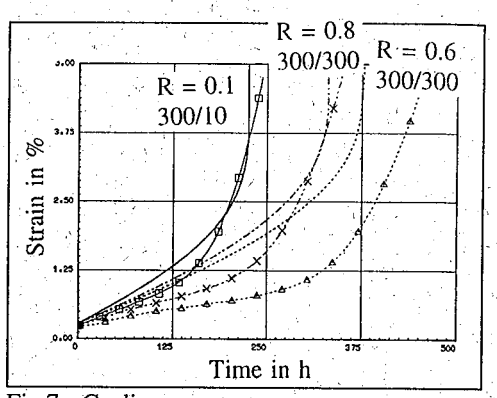

Fig.7. Cyclic creep tests.

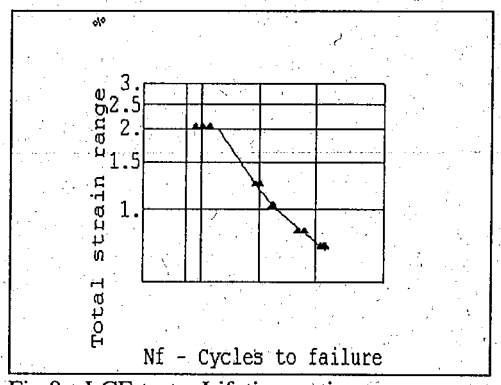

Fig.8. LCF tests. Lifetime estimates.

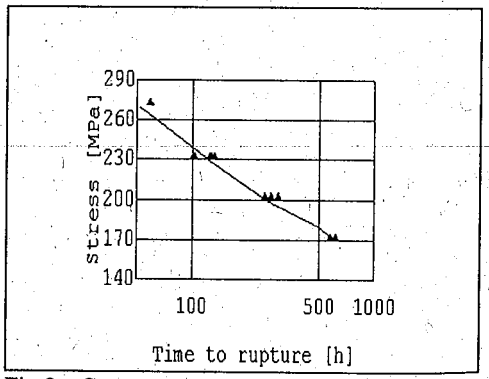

Fig.9. Creep tests. Lifetime estimates.